
The Utility of Decorrelating Colour Spaces in Vector Quantised Variational Autoencoders

Arash Akbarinia Raquel Gil-Rodríguez Alban Flachot Matteo Toscani

Department of General Psychology
Justus-Liebig University, Giessen, Germany
arash.akbarinia@psychol.uni-giessen.de

Abstract

Vector quantised variational autoencoders (VQ-VAE) are characterised by three main components: 1) encoding visual data, 2) assigning k different vectors in the so-called *embedding space*, and 3) decoding the learnt features. While images are often represented in RGB colour space, the specific organisation of colours in other spaces also offer interesting features, e.g. CIE L*a*b* decorrelates chromaticity into opponent axes. In this article, we propose colour space conversion—a simple quasi-unsupervised task—to enforce a network learning structured representations. To this end, we trained several instances of VQ-VAE whose input is an image in one colour space, and its output in another, e.g. from RGB to CIE L*a*b* (in total five colour spaces were considered). We examined the finite embedding space of trained networks in order to disentangle the colour representation in VQ-VAE models. Our analysis suggests that certain vectors encode hue and others luminance information. We further evaluated the quality of reconstructed images at low-level using pixel-wise colour metrics, and at high-level by inputting them to image classification and scene segmentation networks. We conducted experiments in three benchmark datasets: ImageNet, COCO and CelebA. Our results show, with respect to the baseline network (whose input and output are RGB), colour conversion to decorrelated spaces obtains $1-2\Delta E$ lower colour difference and 5-10% higher classification accuracy. We also observed that the learnt embedding space is easier to interpret in colour opponent models.

1 Introduction

Colour is an inseparable component of our conscious visual perception and its objective utility spans over a large set of tasks such as object recognition and scene segmentation [9, 20, 61]. The colour vision sensory system begins in our retina with three types of cone photoreceptors whose sensitivity functions strongly correlate [6, 19]. Horizontal and ganglion cells decorrelate this signal into what is known as colour-opponency before its transmission to the visual cortex [51, 15, 19]. This colour space transformation (from cone excitation to opponency) increases the efficiency of the system in information coding [6, 49, 36]. Correspondingly, opponent colour spaces—like CIE L*a*b*—proved themselves effective in several classical computer vision algorithms [22, 56, 12]. This has been less explored in the modern era of deep-learning except in applications such as style transfer [41, 18] and picture colourisation [8, 34]. Nevertheless, colour opponency appears to be an inherent in deep learning models. Networks trained for high-level visual tasks learn to decorrelate their inputs [48, 16, 24].

A profound grasp on colour neural encoding in deep networks is of great interest, at least, from two standpoints. From a practical perspective, the “ground-truth” of many applications, such as colour transfer [23], colour constancy [7], style transfer [41], computer graphics [5], image denoising [13] and quality assessment [46], is human colour perception. Advancement in these lines requires a

better understanding of colour representation in deep networks. From a theoretical point of view, the neural basis of some aspects of our colour vision, such as unique hues and colour categories, remains to be explained [43, 62, 55]. Insights on whether or how these phenomena emerge in artificial networks can shed light on some of these open questions. Motivated by this, we designed a novel task—colour conversion—to be learnt by Vector Quantised Variational Autoencoders (VQ-VAE) [59]. This simple task helps comprehension of the network’s colour representation by means of comparing the learnt embedding spaces across different instances and colour spaces. We hypothesised a network that, for instance, converts the visual signal from RGB (a space with correlated colour coordinates) to CIE L*a*b (a perceptual colour space with decorrelated coordinates) would exhibit a twofold functionality: better capturing human colour perception and more efficiently conveying colour information in its compressing bottleneck.

The quantification of the latter is more straight forward [52]. We measured the efficiency of colour converting networks in two ways: (i) low-level pixel-wise colour difference to the expected target and (ii) high-level global utility to a visual task. The entanglement of the former to the subjective human perception is best qualitatively analysed. We formalised this by (i) computing the transformations each embedding vector encodes and (ii) measuring its impact on luminance and chromaticity axes of the colour space. Grounded on these analyses, we demonstrate decorrelating colour spaces is beneficial for deep networks in line with the *efficient coding* theory [2, 64]. We present an explanation at the level of embedding vectors according to the *histogram equalisation* technique [45]. Finally, we suggest a novel approach to conceptualise the learnt features of those vectors by a parsimonious linear transformation matrix.

1.1 Related Work

Colour spaces have been investigated in a few empirical studies of deep neural networks (DNNs). Information fusion over several colour spaces improves retinal medical imaging [17]. A similar strategy enhances the robustness of face [37, 33] and traffic light recognition [11, 27]. This has also been explored in predicting eye fixation [54]. Nevertheless, the great majority of the deep learning vision models work with input RGB images.

The theoretical perspective of neural information processing predicts that, because of the constraints on the visual system (i.e. the number of neurons and the metabolic cost of neural activity), visual processing must have an efficient strategy for transmitting information (i.e. *efficient coding* [2, 64]). The idea is to relay receptorial input by encoding it in an efficient and compressed manner to maximise neural resources. An example from the evolution of colour vision is the orthogonalisation of cone responses which yield colour opponent signals [63, 49, 6, 19]. Crucially, efficient coding should match the statistics of the input signals [42]. For instance, colour properties and spatial structures of cells receptive fields in the early visual cortex of the rhesus monkey match very well to the cone excitation from natural scenes [36, 60, 26]. An analogy of *efficient coding* appears in autoencoders due to the narrow nature of their bottlenecks. Due to this constraint, these artificial visual systems must incorporate an efficient strategy to transmit and represent information.

2 Colour Conversion Autoencoders

The ultimate question we would like to answer is how colour gets encoded in deep neural networks (DNNs). At this point, the aim is towards a more generic colour representation rather than describing colour contribution to a specific task. To this end, autoencoders are a suitable tool since their objective is to learn an efficient representation for a set of data in an unsupervised manner [32]. We studied a particular class of these networks—Vector Quantised Variational Autoencoder (VQ-VAE) [59]—due to the discrete nature of its latent embedding space that facilitates the analysis and interpretability of the learnt features. This distinguishes VQ-VAE from other groups of variational encoders [29].

To better address our research question, we propose a novel quasi-unsupervised task of colour conversion: the network’s output colour space is distinct from its input (see Figure 1). A colour space is an arbitrary definition of colours’ organisation in the space [31]. Hence, this simple extension offers the opportunity to learn more about the fundamentals of networks’ internal colour space and whether it underlines a specific set of features. Eventually, we are interested to relate this to human-defined colour spaces with simple mathematical transformation matrices to enhance the interpretability of networks’ internal representation.

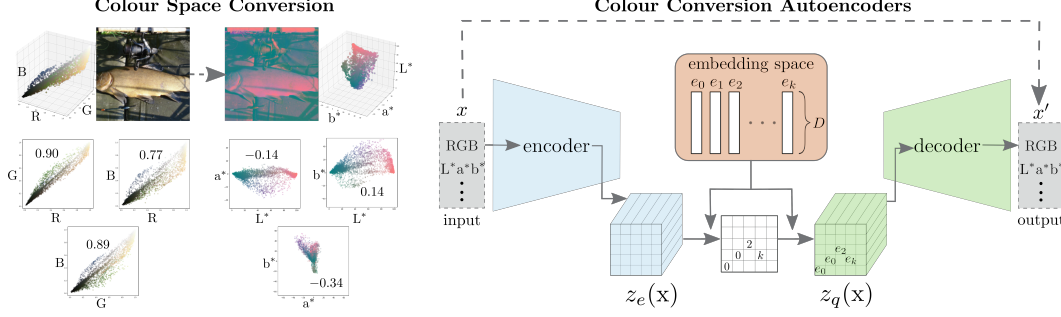


Figure 1: On the left: an exemplary conversion from RGB to CIE L*a*b* colour space. Each image is shown together with its 3D representation of their colours in different axis. On the right: the representation of colour converting VQ-VAE.

2.1 Networks

We focused on Vector Quantised Variational Autoencoder (VQ-VAE) [59]. These networks consist of three main blocks: 1) an encoder that processes the input data x to $z_e(x)$; 2) a latent embedding space $\{e\} \in \mathbb{R}^{K \times D}$, with K vectors of dimensionality D , that maps $z_e(x)$ onto $z_q(x)$ by estimating the nearest vector e_i to $z_e(x)$; 3) a decoder that reconstructs the final output x' with a distribution $p(x|z_q(x))$ over the input data (see the right panel in Figure 1). The loss function is defined as follows,

$$L = \log p(x|z_q(x)) + \|sg[z_e(x)] - e\|_2^2 + \beta \|z_e(x) - sg[e]\|_2^2, \quad (1)$$

where sg denotes the stop gradient computation that is defined as the identity during the forward-propagation, and with zero partial derivatives during the back-propagation to refrain its update. The first term in Eq. 1 corresponds to the reconstruction loss incorporating both encoder and decoder; the second term updates the embedding vectors; and the third term, referred to as the commitment loss, harmonising the encoder and embedding vectors. The parameter $\beta \in \mathbb{R}$ is set to 0.5 in all our experiments.

2.2 Colour Spaces

We studied five three-dimensional colour spaces: RGB, LMS, CIE L*a*b*, DKL and HSV. The RGB colour space is a cubic representation of colours by three additive primaries. RGB is the standard in electronic imaging. The LMS colour space corresponds to the response of human cones (long-, middle-, and short-wavelengths) [21]. The CIE L*a*b* colour space (lightness, red-green and yellow-blue axes) is designed to approximately capture equal perceptual changes [10]. The DKL colour space (Derrington-Krauskopf-Lennie [15]) models the colour opponent responses of rhesus monkeys in the early visual system. The HSV colour space (hue, saturation, value) is a cylindrical representation of RGB cube designed by computer graphics. The intra-axes correlation for RGB and LMS is very high for natural images, hence referred to as *correlated* colour spaces. On the contrary, intra-axes correlations for CIE L*a*b* and DKL are very low, hence referred to as *decorrelated* colour spaces.¹

The input-output to our networks can be in any combination of these colour spaces. Effectively, our VQ-VAE models, in addition to learning efficient representation, must learn the transformation function from their input to output colour space. It is worth considering that the original images in explored datasets are in the RGB format. Therefore, one might expect a slight positive bias towards this colour space given its gamut defines the limits of other colour spaces.

¹We computed these correlations r in all images of ImageNet dataset (hundred-random pixels per image). RGB: $r^{RG} = 0.90$, $r^{RB} = 0.77$, $r^{GB} = 0.89$; LMS: $r^{LM} = 1.00$, $r^{LS} = 0.93$, $r^{MS} = 0.93$; L*a*b*: $r^{L*a*} = -0.14$, $r^{L*b*} = 0.13$, $r^{a*b*} = -0.34$; DKL: $r^{DK} = 0.01$, $r^{DL} = 0.14$, $r^{KL} = 0.61$.

3 Experiments

We trained several instances of VQ-VAEs with distinct sizes of embedding space $\{e\} \in \mathbb{R}^{K \times D}$. The training procedure was identical for all networks: trained with Adam optimiser [28] ($lr = 2 \times 10^{-4}$) for 90 epochs. We used ImageNet dataset [14] for training. This is a visual database of object recognition in real-world images, divided into one thousand categories. The training set contains 1.3 million images. At every epoch, we exposed the network to 100K images of size 224×224 of three colour channels.

To increase the generalisation power of our findings, we evaluated all networks on the validation-set of three benchmark datasets: ImageNet (50K images), COCO (5K images), and CelebA (~20K images). COCO is a large-scale object detection and segmentation dataset [39]. CelebA (CelebFaces Attributes Dataset) [40] contains facial attributes of celebrities. We relied on two classes of evaluation²: low-level [57], to account for the model’s reliability in capturing the local statistics of an image; high-level [4], to assess the model’s capacity in reproducing the global content of an image.

Low-level evaluation – We used the standard colour difference metric CIE ΔE -2000 [53] to measure the pixel-wise performance of networks. The summary of this evaluation is reported in Figure 2. The left panel compares the performance across embedding spaces for RGB-input networks. The high ΔE of *rgb2hsv* pops up at low-dimensionality of the embedding vector ($D = 8$) that might be due to the circular nature of hue. For the smallest and the largest embedding space, we observe no significant differences between the four networks. However, for embedding spaces of 8×8 and 8×128 an advantage appears for networks whose outputs are opponent colour spaces (DKL and CIE L^*a^*b).

The middle and right panels of Figure 2 groups the results into correlated (RGB and LMS) versus decorrelated (DKL and CIE L^*a^*b) colour spaces for both inputs and outputs. HSV is excluded in these analysis due to the aforementioned reason. There is a clear tendency of lower ΔE values for networks whose output colour space is decorrelated. Compare the right columns of each confusion matrix. Overall, the decorrelating networks have an advantage of 2 JND (just-noticeable difference).

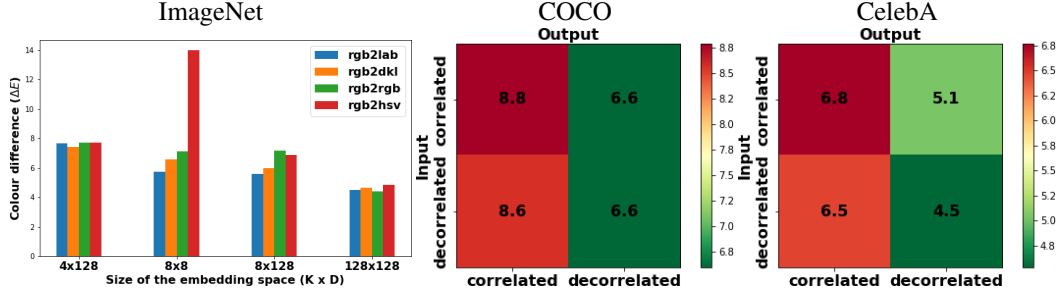


Figure 2: The colour difference (CIE ΔE -2000) between the reconstructed and the original image (the lower the better). Left: results of various sizes of embedding space. Middle and right: pairwise comparison of two groups of input-output colour spaces for the network with $\{e\} \in \mathbb{R}^{8 \times 128}$.

High-level evaluation – Although informative, pixel-wise measures are unable to capture the global content of an image and whether semantic information remains perceptually intact. To account for this limitation, the utility of reconstructed images in a high-level visual task must be measured. We performed a procedure similar to the standard Inception Score [50, 4]. We fed the reconstructed images to two other networks performing the task of object classification (ResNet50 [25]) and scene segmentation (Feature Pyramid Network—FPN [30]). We simply used the pretrained-models of ResNet50 and FPN without any fine-tuning. The evaluation for ResNet50 is the classification accuracy on ImageNet dataset. The evaluation for FPN is the intersection over union (IoU) on COCO dataset. The results for various sizes of embedding space are reported in Figure 3.

The overall trend is much alike for both high-level tasks. The lowest performance occurs for *rgb2hsv* across all embedding spaces. Networks whose output is an opponent colour space systematically perform better than *rgb2rgb*, with an exception for the largest embedding space (128×128). The

²For reproduction, the source code and all experimental data are available in our GitHub: <https://github.com/ArashAkbarinia/DecomposeNet>.

comparison of the smallest embedding space (4×128) across Figures 2 and 3 demonstrates the importance of high-level evaluation. Although no difference emerges for the measure of ΔE , the classification and segmentation metrics are substantially influenced by the quality of the reconstructed images in those four VQ-VAEs.

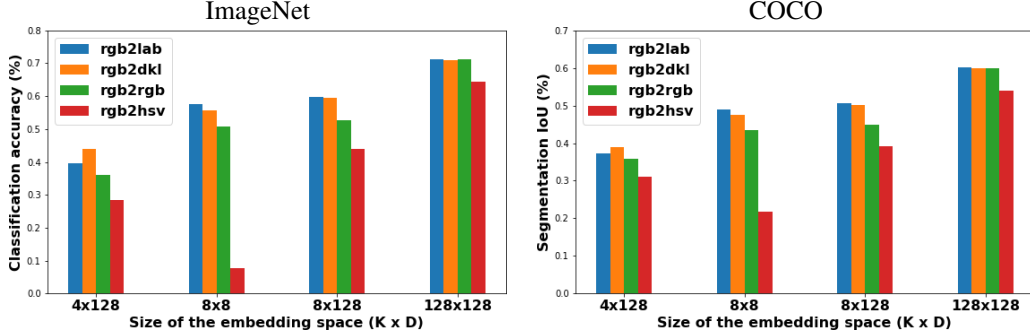


Figure 3: High-level visual task evaluation. Left: ResNet50’s classification accuracy on reconstructed images of ImageNet. Right: FPNS’s segmentation IoU on reconstructed images of COCO.

To thoroughly examine the effect observed above, networks whose output is an opponent colour space perform better than the baseline *rgb2rgb* models, we performed a pairwise comparison of all combinations of input and output colour spaces. The results are reported in Figure 4. The model executing the *rgb2lab* colour conversion obtains the highest performance across both datasets and embedding space capacity (the top row). Overall, we observe a clear advantage for networks whose output is a decorrelated colour space (the bottom row). This suggests the neural information processing is optimised by opponency, in line with the *efficient coding* theory [2, 64].

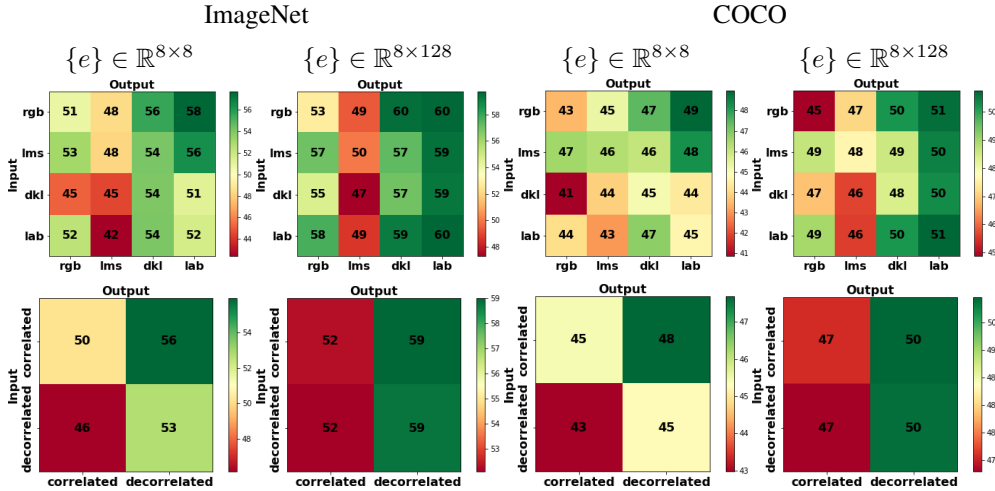


Figure 4: Pairwise comparison of correlated (RGB and LMS) versus decorrelated (DKL and L*a*b) input-output colour spaces of VQ-VAEs. ImageNet metric: accuracy; COCO: IoU.

3.1 Explaining the Performance Advantage

Networks whose output is a decorrelated colour space are more efficient. Understanding its cause is of great interest [38]. We hypothesised that the *orthogonality* [6] of networks’ embedding vectors would explain this effect. Nevertheless, no significant correlation emerged in this respect. We further explored the frequency of each embedding vector being used in the latent representation of images. Our hypothesis is: an efficient system distributes its encoding across all resources instead of heavily relying on a few components [35]. We measured this by computing the histogram of embedding vectors across all images ImageNet (50K) and COCO (5K). A zero standard deviation in frequency of

selected vectors means an equal utilisation of all embedding vectors. In Figure 5, we have plotted the error rate as a function of this measure. A significant correlation emerges in both datasets, suggesting a more uniform contribution of embedding vectors in VQ-VAEs enhances their visual information representation. This matches the neural model of histogram equalisation [45] and is consistent with the *efficient coding* theory for the biological visual system. In fact, to overcome the neurons restricted range of responses, *efficient coding* could be achieved by encoding the input so that all response levels are used with equal frequency. If so, the encoded information is maximised because the information channel (i.e. the neuron) achieves its maximum entropy. Such coding can be achieved by computing responses from the cumulative probability function for the input distribution, so that equal output excursions correspond to equal probabilities of input. This mapping was found to take place in biological neural systems like neurons in the fly’s compound eye [35].

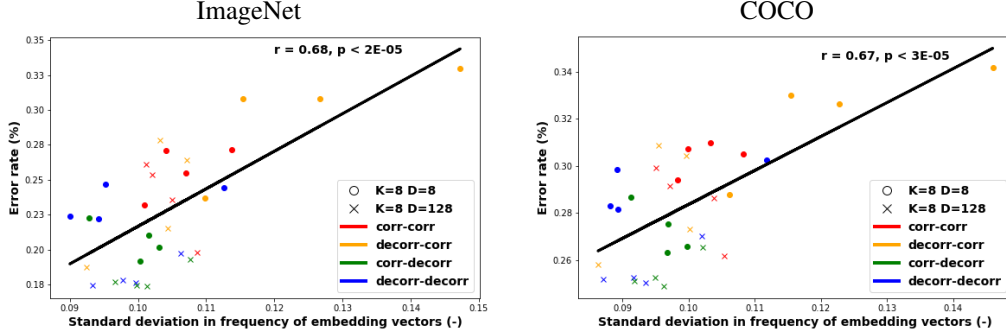


Figure 5: Error rate as a function of the difference in frequency of selected vectors in the embedding space. A value of zero in the x -axis indicates all embedding vectors are equally used by the model. Higher values of x indicate that the model relies heavily on certain vectors.

4 Interpreting the Embedding Space

Comprehension of the features learnt by a DNN remains a great challenge to the entire community [38]. Generative models and in particular variational autoencoders are no exceptions. Many works have focused on visual exploration of DNN’s latent spaces. Interpolation or arithmetic operations on learnt latent features can reveal some meaningful and interpretable structure of these spaces [47, 3, 27]. In practice, however, these approaches require explicit human supervision, a cumbersome task due to the often large dimensionality of the latent space. Here, we borrowed the “lesion” technique, commonly practised in the neuroscience community [58], and applied it to the embedding space by silencing one vector at a time (i.e. setting its weights to zero). A similar approach has revealed contrast kernels in DNNs [1]. To measure the consequences of vectors’ lesion, we quantified the chromatic shifts (in CIE $L^*a^*b^*$) between the reconstructed image of full embedding space and lesion one. The differences computed for all pixels over a hundred random images from the COCO dataset are illustrated in Figure 6.

This analysis provides an intuitive interpretation of some of the embedding vectors. For instance, the e_0 lesion in the *rgb2dkl* network only impacts the chromatic axes. The direction of its shift implies pixels in the first quadrant of the chromaticity plane are effected (i.e. red pixels, see a^*b^* plane in panel E of Figure 8). The e_1 vector of the same network appears to largely encode the luminance information. The e_2 vector predominantly influences the blue pixels (negative direction in the b^* axis). Intrigued by this interpretation, we sampled from the embedding space an example where all pixels are of the same vector index. An RGB visualisation of this technique’s output is illustrated in Figure 7. Naturally, each vector encodes more than this simple reconstructed hues. However, the colour of these hues match the direction of shifts in Figure 6 and both together offer a perspective on colour representation in these VQ-VAEs.

To better conceptualise the effect of vector lesion, we have illustrated the *rgb2dkl*’s reconstructions for three exemplary images in Figure 8. Panel A corresponds to the full embedding space and panels B–D show examples of reconstructions with distinct vector lesions causing clear perceptual effects. In B, the lightness of very bright pixels is reduced (attend pixels outside the window and around

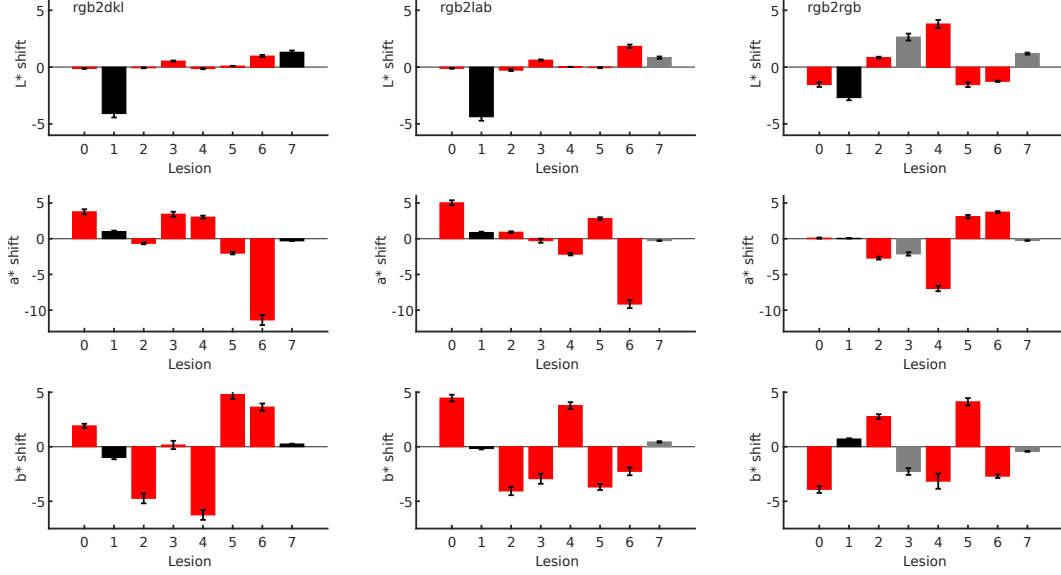


Figure 6: Average chromatic shifts in CIE $L^*a^*b^*$ colour space for each vector lesion. Numbers in the x-axis denote the indices of the embedding vectors. All networks are of $\{e\} \in \mathbb{R}^{8 \times 128}$. Grey bars indicate those vectors that predominantly impact the luminance channel.



Figure 7: The reconstruction output by selecting a single vector of the entire embedding space. All models are of $\{e\} \in \mathbb{R}^{8 \times 128}$.

light bulbs) while changes of chromaticity are unnoticeable. Contrary to this, in C & D, colour is drastically modified with reddish and blueish pixels, respectively, turning achromatic.

We hypothesised that the changes induced by a lesion, presented in Figure 6, could be approximated by a linear transformation mapping the pixel distribution of the full reconstruction onto the lesion image. To compute these transformations, we used a multi-linear regression to find the best linear fit for the 1% of pixels most affected with a lesion. The resulting 3×3 matrix is a linear transformation in the three-dimensional CIE $L^*a^*b^*$ colour space (see the right side of Figure 8). Lesions are excellently approximated by a linear transformation: on average accounting for 97% of the total variance in the lesion effect (the lowest bound was 86%).

We diagonalised those resulting matrices to simplify their interpretations. The relative norms of the eigenvalues are indicative of the geometrical properties of the transformation matrices. For instance, the presence of at least one eigenvalue equal to zero specifies the extreme case of a singular matrix, corresponding to a linear transformation projecting a three-dimensional space onto lower dimensions. We quantified this by defining a singularity index [44]. Consider a transformation matrix T approximating the lesion effect on the image colour distribution. Let λ_1 , λ_2 and λ_3 be the three eigenvalues of T , such that $\|\lambda_1\| > \|\lambda_2\| > \|\lambda_3\|$. The singularity index is defined as: $SI = 1 - \frac{\lambda_3}{\lambda_1}$.

On the right side of Figure 8, we have illustrated the result of applying these linear transformations in CIE $L^*a^*b^*$ coordinates. Panel E corresponds to the full RGB cube (essentially the $L^*a^*b^*$ planes limited by RGB gamut). In panels F–H the very same points are plotted transformed by the matrix modelled from the lesion of that vector. This visualisation offers an intuitive interpretation of the embedding space. In the images of the second row (panel B), contrast in bright pixels is reduced and colour is little modified. We can observe this in its corresponding $L^*a^*b^*$ planes (e.g. attend the a^*b^* plane in F where the overall chromaticity structure is retained). In C, red pixels turn grey also evident in its corresponding $L^*a^*b^*$ planes (panel F) where red coordinates are collapsed. These features qualitatively match well to those reported in Figures 7 and 6. The singularity index also adequately captures the essence of these transformations. On the one hand, the low value of SI in F suggests the

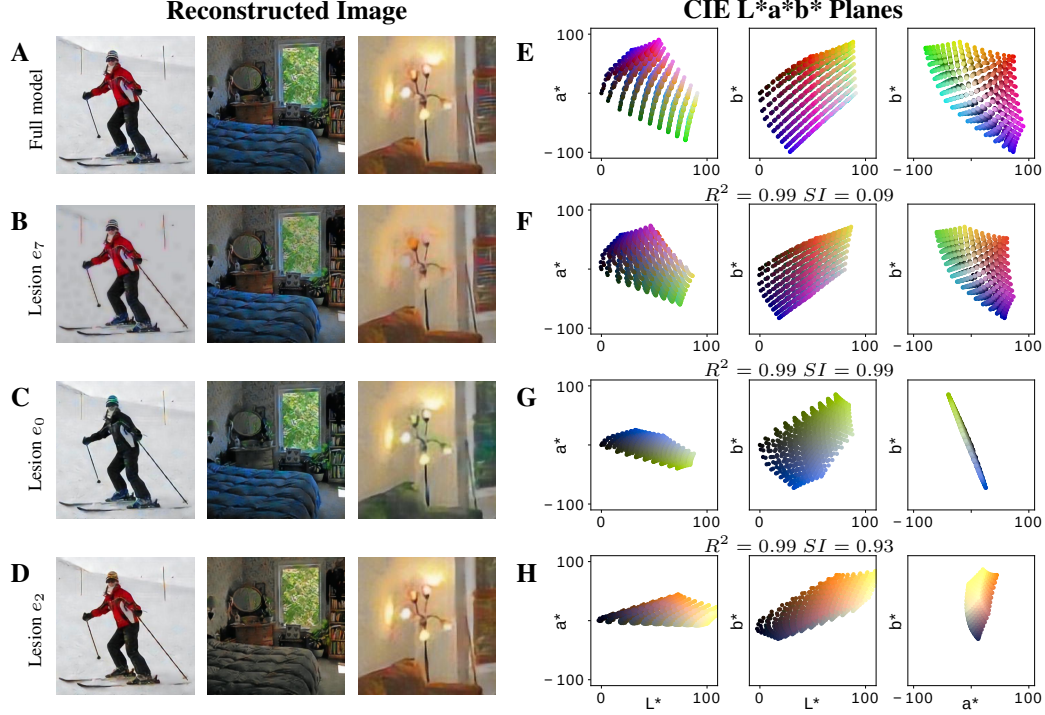


Figure 8: Visualisation of the lesion effect for the *rgb2dkl* VQ-VAE $\{e\} \in \mathbb{R}^{8 \times 128}$. On the left, images reconstructed by **A**: the full model; **B-D**: the lesion embedding space. On the right, scatter plots in CIE $L^*a^*b^*$ coordinates of **E**: the entire RGB cube; **F-H**: the RGB cube after applying the linear transformations modelled by each lesion.

global shape of colour space is retained while its volume is reduced. On the other hand, high values of *SI* in panels G and H indicate the near collapse of a dimension.

The average *SI* is very similar for *rgb2dkl*, *rgb2lab* and *rgb2rgb*, 0.75, 0.73 and 0.72 respectively. Thresholding these indices distinguishes two family of transformation matrices T . The *singular* group with $SI \geq 0.90$ indicating a lesion impact of *at least* ten times larger along one dimension of the colour space. The *homogeneous* group with $SI \leq 0.10$ indicating a lesion of uniform impact across all colour dimension with modulation in their contrast. Following these criteria, three of eight transformation matrices classify as *singular* in all three colour converting networks. We observed only one *homogeneous* matrix in the *rgb2dkl* network (i.e. e_7 depicted in the second row of Figure 8).

To summarise, performing the lesion technique on vectors of the VQ-VAE’s embedding space presents interesting insights. Colour changes induced by these lesions can be faithfully modelled with parsimonious linear transformations. Studying these simple matrices offers an explicit understanding of lesions effect. In turn, this can shed light on colour representation in VQ-VAE models and open a promising line of investigation to decipher how visual information is encoded in generative models.

5 Conclusion

In this article, we introduced a simple quasi-unsupervised task—*colour conversion*—for variational autoencoders. The comparison across several colour spaces suggests a network with a decorrelated colour space as its output exhibits an advantage in terms of capturing local and global features. We offered an explanation for this within the framework of *efficient coding* [2, 64] and *histogram equalisation* [45]. These principles are not specific to autoencoders and could be applicable to a larger family of deep learning models. We proposed a set of methods to interpret the embedding space of VQ-VAEs. Many of the constituent vectors manifest a clear effect along one colour direction.

We showed the vectors’ influence could be modelled by *parsimonious linear transformations*. This is a powerful tool with great potentials to enhance the interpretability of latent spaces in general.

Acknowledgement

This study was funded by Deutsche Forschungsgemeinschaft SFB/TRR 135.

References

- [1] Arash Akbarinia and Raquel Gil-Rodríguez. Deciphering image contrast in object classification deep networks. *Vision Research*, 173:61–76, 2020.
- [2] Horace B Barlow. Possible principles underlying the transformation of sensory messages. In *Sensory communication*, pages 217–234, Cambridge, UK, 1961. MIT Press.
- [3] Piotr Bojanowski, Armand Joulin, David Lopez-Paz, and Arthur Szlam. Optimizing the latent space of generative networks. *arXiv preprint arXiv:1707.05776*, 2017.
- [4] Ali Borji. Pros and cons of gan evaluation measures. *Computer Vision and Image Understanding*, 179:41–65, 2019.
- [5] M. Bratkova, S. Boulos, and P. Shirley. orgb: A practical opponent color space for computer graphics. *IEEE Computer Graphics and Applications*, 29(1):42–55, 2009.
- [6] Gershon Buchsbaum and Gottschalk Allan. Trichromacy, opponent colours coding and optimum colour information transmission in the retina. *Proceedings of the Royal society of London. Series B. Biological sciences*, 220(1218):89–113, 1983.
- [7] Ayan Chakrabarti. Color constancy by learning to predict chromaticity from luminance. In *Advances in Neural Information Processing Systems*, pages 163–171, 2015.
- [8] Zezhou Cheng, Qingxiong Yang, and Bin Sheng. Deep colorization. In *Proceedings of the IEEE International Conference on Computer Vision*, pages 415–423, 2015.
- [9] M Chirimuuta et al. The uses of colour vision: Ornamental, practical, and theoretical. *Minds and Machines*, 25(2):213–229, 2015.
- [10] CIE. Recommendations on uniform color spaces, color-difference equations, psychometric color terms. Paris:CIE, 1978.
- [11] Dan CireşAn, Ueli Meier, Jonathan Masci, and Jürgen Schmidhuber. Multi-column deep neural network for traffic sign classification. *Neural networks*, 32:333–338, 2012.
- [12] Ivo M Creusen, Rob GJ Wijnhoven, Ernst Herbschleb, and PHN de With. Color exploitation in hog-based traffic sign detection. In *2010 IEEE International Conference on Image Processing*, pages 2669–2672. IEEE, 2010.
- [13] Kostadin Dabov, Alessandro Foi, Vladimir Katkovnik, and Karen Egiazarian. Image denoising by sparse 3-d transform-domain collaborative filtering. *IEEE transactions on image processing : a publication of the IEEE Signal Processing Society*, 16:2080–95, 09 2007.
- [14] Jia Deng, Wei Dong, Richard Socher, Li-Jia Li, Kai Li, and Li Fei-Fei. Imagenet: A large-scale hierarchical image database. In *2009 IEEE conference on computer vision and pattern recognition*, pages 248–255. Ieee, 2009.
- [15] Andrew M Derrington, John Krauskopf, and Peter Lennie. Chromatic mechanisms in lateral geniculate nucleus of macaque. *The Journal of physiology*, 357(1):241–265, 1984.
- [16] Alban Flachot and Karl R Gegenfurtner. Processing of chromatic information in a deep convolutional neural network. *JOSA A*, 35(4):B334–B346, 2018.
- [17] Huazhu Fu, Boyang Wang, Jianbing Shen, Shanshan Cui, Yanwu Xu, Jiang Liu, and Ling Shao. Evaluation of retinal image quality assessment networks in different color-spaces. In *International Conference on Medical Image Computing and Computer-Assisted Intervention*, pages 48–56. Springer, 2019.
- [18] Leon A Gatys, Alexander S Ecker, Matthias Bethge, Aaron Hertzmann, and Eli Shechtman. Controlling perceptual factors in neural style transfer. In *Proceedings of the IEEE Conference on Computer Vision and Pattern Recognition*, pages 3985–3993, 2017.
- [19] Karl Gegenfurtner and Daniel C Kiper. Color vision. *Annual review of neuroscience*, 26:181–206, 2003.

- [20] Karl R Gegenfurtner and Jochem Rieger. Sensory and cognitive contributions of color to the recognition of natural scenes. *Current Biology*, 10(13):805–808, 2000.
- [21] Karl R Gegenfurtner and Lindsay A Sharpe. *Color vision*. Cambridge University Press, Cambridge, UK, 1999.
- [22] Theo Gevers and Harro Stokman. Robust histogram construction from color invariants for object recognition. *IEEE transactions on pattern analysis and machine intelligence*, 26(1):113–118, 2004.
- [23] Raquel Gil-Rodríguez, Javier Vazquez-Corral, and Marcelo Bertalmío. Color matching images with unknown non-linear encodings. *IEEE Transactions on Image Processing*, 29:4435–4444, 2020.
- [24] Ethan Harris, Daniela Mihai, and Jonathon Hare. Spatial and colour opponency in anatomically constrained deep networks. *arXiv preprint arXiv:1910.11086*, 2019.
- [25] Kaiming He, Xiangyu Zhang, Shaoqing Ren, and Jian Sun. Deep residual learning for image recognition. In *Proceedings of CVPR*, pages 770–778, 2016.
- [26] Aapo Hyvärinen and Patrik Hoyer. Emergence of phase-and shift-invariant features by decomposition of natural images into independent feature subspaces. *Neural computation*, 12(7):1705–1720, 2000.
- [27] Hyun-Koo Kim, Ju H Park, and Ho-Youl Jung. An efficient color space for deep-learning based traffic light recognition. *Journal of Advanced Transportation*, 2018, 2018.
- [28] Diederik P Kingma and Jimmy Ba. Adam: A method for stochastic optimization. *arXiv preprint arXiv:1412.6980*, 2014.
- [29] Diederik P Kingma and Max Welling. Auto-encoding variational bayes. *arXiv preprint arXiv:1312.6114*, 2013.
- [30] Alexander Kirillov, Kaiming He, Ross Girshick, Carsten Rother, and Piotr Dollár. Panoptic segmentation. In *Proceedings of the IEEE conference on computer vision and pattern recognition*, pages 9404–9413, 2019.
- [31] JJ Koenderink and Andrea J van Doorn. *Perspectives on colour space*. Oxford University, 2003.
- [32] Mark A Kramer. Nonlinear principal component analysis using autoassociative neural networks. *AIChE journal*, 37(2):233–243, 1991.
- [33] Kaouthar Larbi, Wael Ouarda, Hassen Drira, Boulbaba Ben Amor, and Chokri Ben Amar. Deepcolorfasd: Face anti spoofing solution using a multi channeled color spaces cnn. In *2018 IEEE International Conference on Systems, Man, and Cybernetics (SMC)*, pages 4011–4016. IEEE, 2018.
- [34] Gustav Larsson, Michael Maire, and Gregory Shakhnarovich. Learning representations for automatic colorization. In *European Conference on Computer Vision*, pages 577–593. Springer, 2016.
- [35] Simon Laughlin. A simple coding procedure enhances a neuron’s information capacity. *Zeitschrift für Naturforschung c*, 36(9-10):910–912, 1981.
- [36] Te-Won Lee, Thomas Wachtler, and Terrence J Sejnowski. Color opponency constitutes a sparse representation for the chromatic structure of natural scenes. In *Advances in Neural Information Processing Systems*, pages 866–872, 2001.
- [37] Wei Li, Rui Zhao, Tong Xiao, and Xiaogang Wang. Deepreid: Deep filter pairing neural network for person re-identification. In *Proceedings of the IEEE conference on computer vision and pattern recognition*, pages 152–159, 2014.
- [38] Timothy P Lillicrap and Konrad P Kording. What does it mean to understand a neural network? *arXiv preprint arXiv:1907.06374*, 2019.
- [39] Tsung-Yi Lin, Michael Maire, Serge Belongie, James Hays, Pietro Perona, Deva Ramanan, Piotr Dollár, and C Lawrence Zitnick. Microsoft coco: Common objects in context. In *European conference on computer vision*, pages 740–755. Springer, 2014.
- [40] Ziwei Liu, Ping Luo, Xiaogang Wang, and Xiaoou Tang. Deep learning face attributes in the wild. In *Proceedings of the IEEE international conference on computer vision*, pages 3730–3738, 2015.

- [41] Fujun Luan, Sylvain Paris, Eli Shechtman, and Kavita Bala. Deep photo style transfer. In *Proceedings of the IEEE Conference on Computer Vision and Pattern Recognition*, pages 4990–4998, 2017.
- [42] Vivienne L Ming and Lori L Holt. Efficient coding in human auditory perception. *The Journal of the Acoustical Society of America*, 126(3):1312–1320, 2009.
- [43] C Alejandro Parraga and Arash Akbarinia. Nice: A computational solution to close the gap from colour perception to colour categorization. *PloS one*, 11(3):e0149538, 2016.
- [44] David L Philipona and J Kevin O’reagan. Color naming, unique hues, and hue cancellation predicted from singularities in reflection properties. *Visual neuroscience*, 23(3-4):331–339, 2006.
- [45] W Pratt. Digital image processing wiley-interscience, 2007.
- [46] J. Preiss, F. Fernandes, and P. Urban. Color-image quality assessment: From prediction to optimization. *IEEE Transactions on Image Processing*, 23(3):1366–1378, 2014.
- [47] Alec Radford, Luke Metz, and Soumith Chintala. Unsupervised representation learning with deep convolutional generative adversarial networks. *arXiv preprint arXiv:1511.06434*, 2015.
- [48] Ivet Rafegas and Maria Vanrell. Color encoding in biologically-inspired convolutional neural networks. *Vision research*, 151:7–17, 2018.
- [49] Daniel L Ruderman, Cronin W Thomas, and Chiao Chuan-Chin. Statistics of cone responses to natural images: implications for visual coding. *JOSA A*, 15(8):2036–2045, 1998.
- [50] Tim Salimans, Ian Goodfellow, Wojciech Zaremba, Vicki Cheung, Alec Radford, and Xi Chen. Improved techniques for training gans. In *Advances in neural information processing systems*, pages 2234–2242, 2016.
- [51] Peter H Schiller and Joseph G Malpeli. Properties and tectal projections of monkey retinal ganglion cells. *Journal of Neurophysiology*, 40(2):428–445, 1977.
- [52] Michael W Schwarz, William B Cowan, and John C Beatty. An experimental comparison of rgb, yiq, lab, hsv, and opponent color models. *ACM Transactions on Graphics (TOG)*, 6(2):123–158, 1987.
- [53] Gaurav Sharma, Wencheng Wu, and Edul N Dalal. The ciede2000 color-difference formula: Implementation notes, supplementary test data, and mathematical observations. *Color Research & Application*, 30(1):21–30, 2005.
- [54] Chengyao Shen, Xun Huang, and Qi Zhao. Predicting eye fixations on webpage with an ensemble of early features and high-level representations from deep network. *IEEE Transactions on Multimedia*, 17(11):2084–2093, 2015.
- [55] Katarzyna Siuda-Krzywicka, Marianna Boros, Paolo Bartolomeo, and Christoph Witzel. The biological bases of colour categorisation: From goldfish to the human brain. *Cortex*, 2019.
- [56] Harro Stokman and Theo Gevers. Selection and fusion of color models for image feature detection. *IEEE transactions on pattern analysis and machine intelligence*, 29(3):371–381, 2007.
- [57] Lucas Theis, Aäron van den Oord, and Matthias Bethge. A note on the evaluation of generative models. *arXiv preprint arXiv:1511.01844*, 2015.
- [58] Avinash R Vaidya, Maia S Pujara, Michael Petrides, Elisabeth A Murray, and Lesley K Fellows. Lesion studies in contemporary neuroscience. *Trends in cognitive sciences*, 2019.
- [59] Aaron van den Oord, Oriol Vinyals, et al. Neural discrete representation learning. In *Advances in Neural Information Processing Systems*, pages 6306–6315, 2017.
- [60] J Hans Van Hateren and Arjen van der Schaaf. Independent component filters of natural images compared with simple cells in primary visual cortex. *Proceedings of the Royal Society of London B: Biological Sciences*, 265(1394):359–366, 1998.
- [61] Felix A Wichmann, Lindsay A Sharpe, and Karl R Gegenfurtner. The contributions of color to recognition memory for natural scenes. *Journal of Experimental Psychology: Learning, Memory, and Cognition*, 28(3):509, 2002.
- [62] Christoph Witzel and Karl R Gegenfurtner. Color perception: Objects, constancy, and categories. *Annual Review of Vision Science*, 2018.

- [63] Qasim Zaidi. Decorrelation of l-and m-cone signals. *JOSA A*, 14(12):3430–3431, 1997.
- [64] Li Zhaoping. Theoretical understanding of the early visual processes by data compression and data selection. *Network: computation in neural systems*, 17(4):301–334, 2006.

A Qualitative Comparison

Along with the quantitative evaluations reported in the manuscript, the benefits of utilising a decorrelated colour space for the network’s output can be appreciated qualitatively (see Figure 9). These are representative samples from the COCO dataset [39]. The Jupyter-Notebook scripts our GitHub provide more examples³. Overall, the *rgb2dkl* and *rgb2lab* VQ-VAEs generate more coherent images. For instance, in the first row of Figure 9, the *rgb2rgb* output contains a large amount of artefacts on walls and ceilings. In contrast, the output of *rgb2dkl* and *rgb2lab* are sharper.

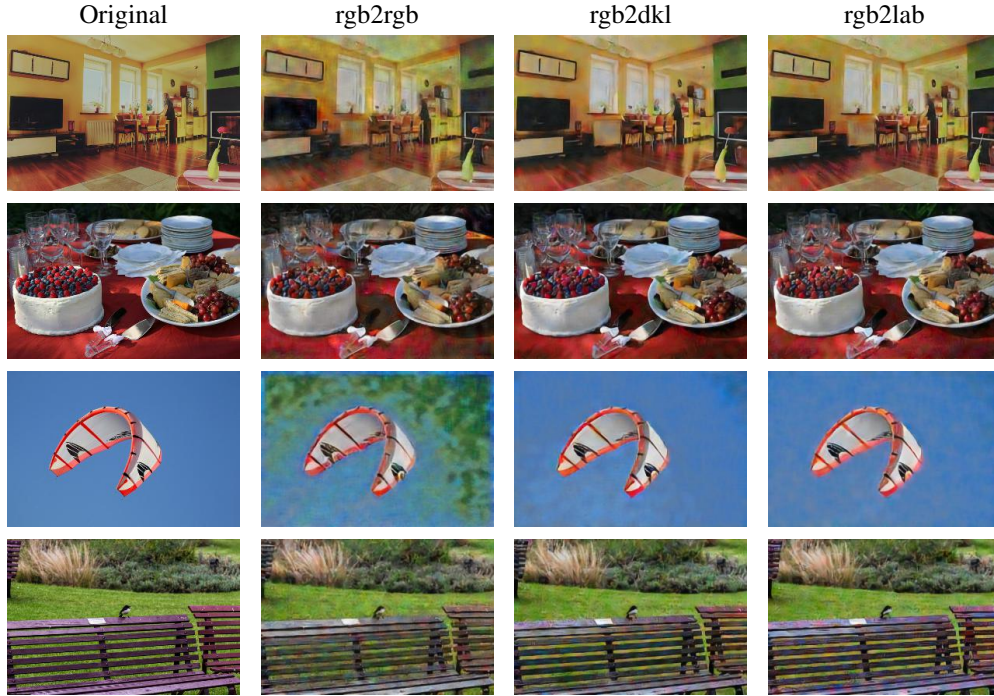


Figure 9: Qualitative comparison of three VQ-VAEs of $K=8$ and $D=128$.

B Quantitative Comparison

The qualitative intuitions from the pictures above match very well the computed quantitative metrics.

B.1 Low-level Pixel-wise

Figure 10 compares the colour difference metric of four colours converting VQ-VAEs with various sizes of embedding space. The results for ImageNet and COCO are very similar. The benefit of using DKL or CIE $L^*a^*b^*$ colour spaces for the network’s output appears when the embedding space contains eight vectors (i.e. 8×8 and 8×128). In high-level visual task evaluation (Figure 13) the benefit of these two colour spaces is also evident for the 4×128 network. This effect disappears for the largest networks (128×128). Perhaps, the benefit of decorrelated colour space vanishes with abundant of computation resources. To resolve this, we propose a psychophysical experiment in which participants must judge the quality of generated images for these networks.

³The weights of all trained networks and image outputs of lesion study are publicly available for interested readers in our GitHub: <https://github.com/ArashAkbarinia/DecomposeNet>.

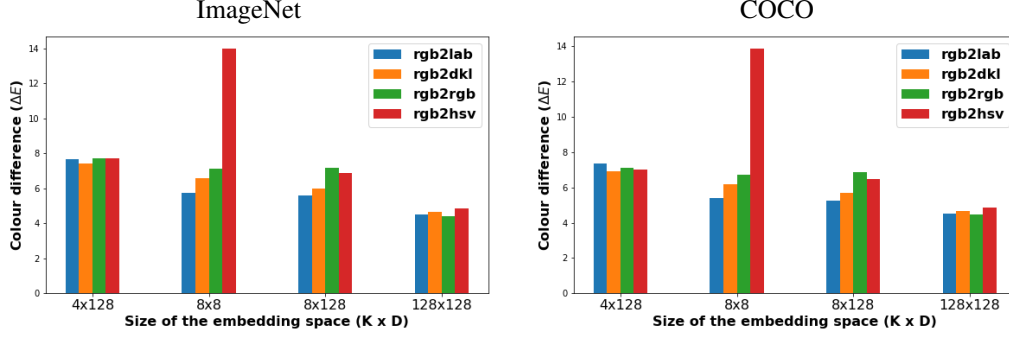


Figure 10: The colour difference (CIE ΔE -2000) between the reconstructed and the original image (the lower the better).

The first rows of Figures 11 and 12 illustrate a pair-wise comparison of conversion among four colour spaces and the second rows group them into correlated and decorrelated colour spaces. Networks whose outputs are a decorrelated colour space obtain lower colour difference (more than $2\Delta E$).

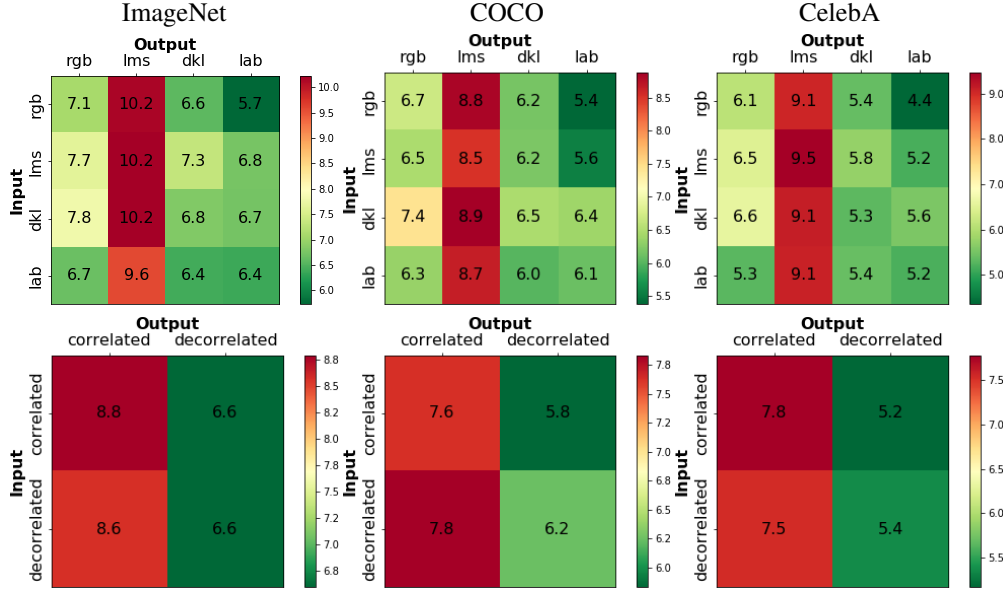


Figure 11: CIE ΔE -2000 pairwise comparison of correlated (RGB and LMS) versus decorrelated (DKL and L*a*b) input-output colour spaces for VQ-VAEs of $K=8$ and $D=8$.

B.2 High-level Visual Tasks

Figure 13 compares high-level metrics of four colour converting VQ-VAEs with various sizes of embedding space. The results for ImageNet and COCO are very similar. The benefit of using DKL or CIE L*a*b* colour spaces for the network’s output appears in all except for the largest embedding space (128×128). This suggests that colour opponency might be related to the scarcity of the computational resources a visual system faces, in line with *efficient coding* [2, 64].

The first rows of Figure 14 illustrates a pair-wise comparison of conversion among four colour spaces and the second row group them into correlated and decorrelated colour spaces. Networks whose outputs are a decorrelated colour space on average obtain higher classification accuracy and segmentation IoU (about 5%). Within this group the *rgb2lab* tends to systematically achieves higher performance in comparison to the *rgb2dkl*. Although the difference is quite small this is interesting to

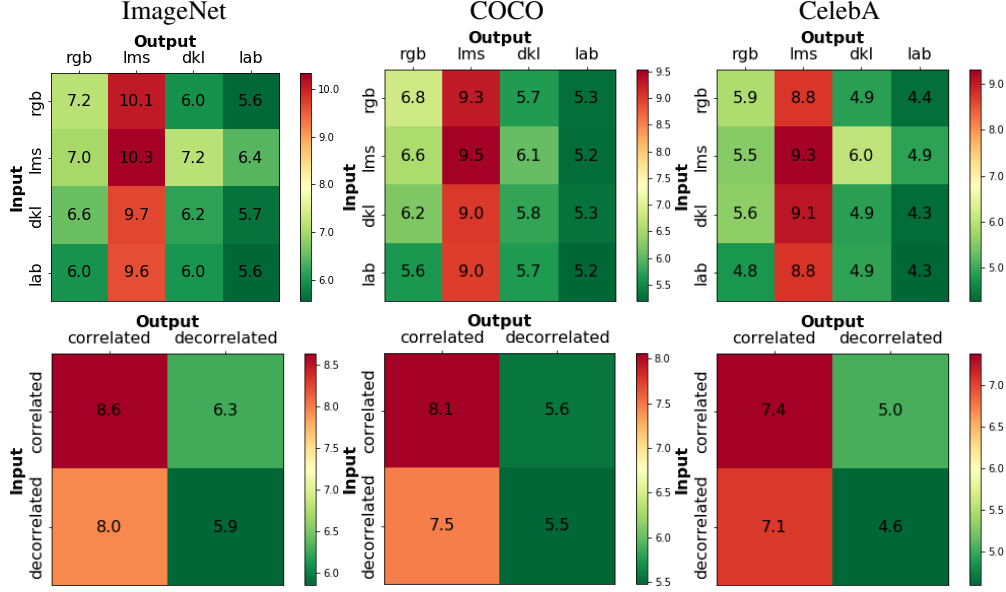


Figure 12: CIE ΔE -2000 pairwise comparison of correlated (RGB and LMS) versus decorrelated (DKL and L*a*b) input-output colour spaces for VQ-VAEs of $K=8$ and $D=128$.

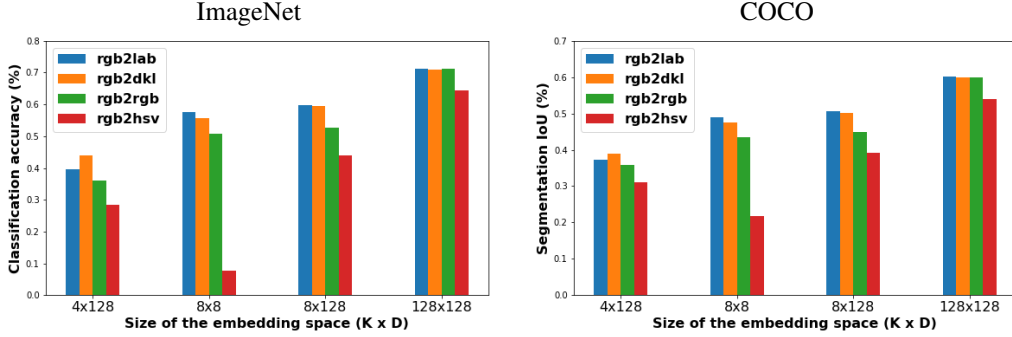


Figure 13: High-level visual task evaluation. Left: ResNet50's classification accuracy on reconstructed images of ImageNet. Right: FPNS's segmentation IoU on reconstructed images of COCO.

explore the reason behind. Perhaps the nonlinear operation in the luminance channel of CIE L*a*b* is the root cause of this effect.

C Interpreting the Embedding Space

In order to decipher the role of each embedding vector we explored and developed a set of techniques.

C.1 Embedding Vector's Hue

In order to visualise the information each vector encodes, we sampled from the embedding space an example where all pixels are of the same vector index. In particular, we report the results for $\{e\} \in \mathbb{R}^{K \times D}$ with $K = 8$ and $D = 8, 128$; in all the 16 possible combinations with input/output $\{rgb, lms, dkl, lab\}$.

Figure 15 shows the reconstructed images for all network combinations with embedding space $\{e\} \in \mathbb{R}^{8 \times 128}$. In each row, the input colour space is the same. In each column, the output colour space is the same. An interesting column-wise feature appears. Networks with an identical colour space output share a similar set of hues arranged in different orders. The order within the embedding

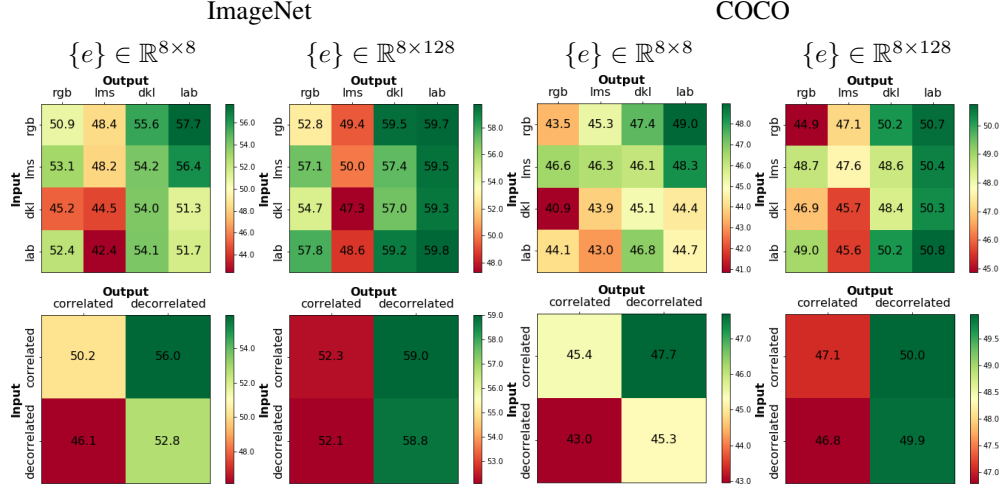


Figure 14: Pairwise comparison of correlated (RGB and LMS) versus decorrelated (DKL and L*a*b) input-output colour spaces of VQ-VAEs. Metric is accuracy for ImageNet and IoU for COCO.

space of VQ-VAEs is arbitrary and changing it does not impact the network’s output. This is an interesting phenomenon suggesting the colour representation in network’s embedding space is an attribute of its output colour space. This is less evident in *rgb2rgb* networks and networks of smaller embedding space, $\{e\} \in \mathbb{R}^{8 \times 8}$, presented in Figure 16. This is an exciting line of investigation for feature studies to systematically explore whether the concept of unique hues and colour categories [62, 55] emerge in machine colour representation.

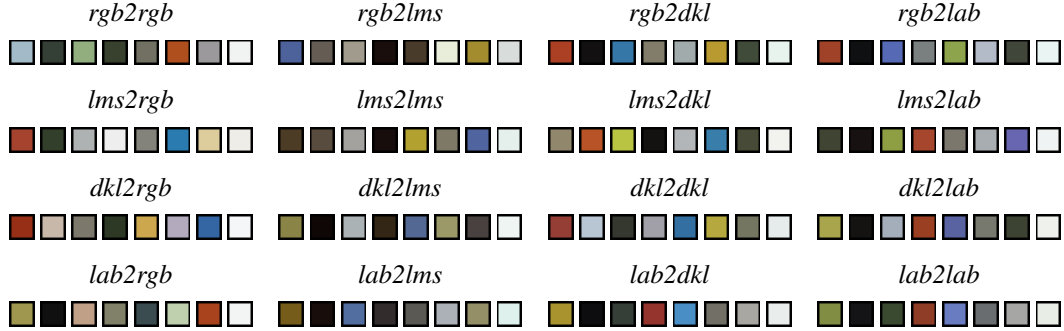


Figure 15: The reconstruction output by selecting a single vector of the entire embedding space. All models are VQ-VAE of $K=8$ and $D=128$.

C.2 Linear Modelling of Vector Lesions

In order to understand the features learnt by the colour conversion networks, we exercised the “lesion” technique. It consists of silencing the embedding space’s vectors one at a time. We explored whether a vector lesion can be modelled by a simple linear transformation. We estimated the transformation matrix that maps the pixel distribution of the full reconstruction onto the lesion image (refer to Section 4 in the manuscript). To our surprise, this simple parsimonious modelling can capture a large portion of the vector’s encoding. We present qualitative results for VQ-VAEs with $K = 8$ and $D = 128$ in the colour conversion networks *rgb2dkl* (Figure 17), *rgb2lab* (Figure 18) and *rgb2rgb* (Figure 19).

The top row of Figure 17 illustrated three examples from the COCO dataset reconstructed with the full model of *rgb2dkl*. The following rows depict the reconstruction output of lesion technique exercised on each embedding vector e_i (the “Lesion output” column), alongside with the linear modelling estimation (the “Linear model” column) obtained by applying the linear transformation to the full reconstructed image. On the bottom right corner, we have reported the fitness of the mode, correlation

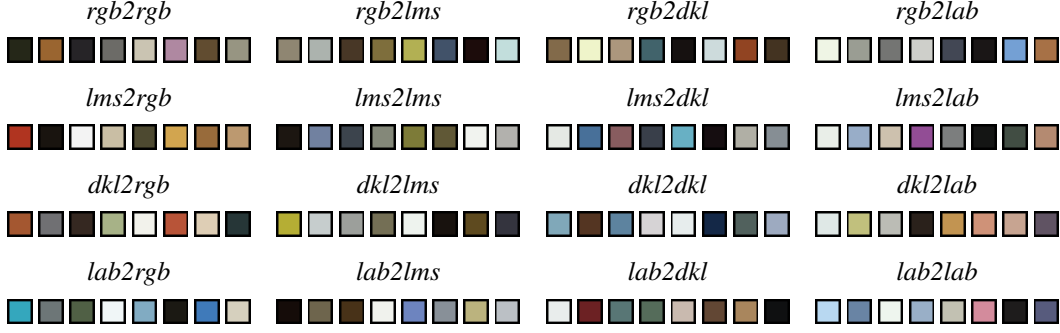


Figure 16: The reconstruction output by selecting a single vector of the entire embedding space. All models are VQ-VAE of $K=8$ and $D=8$.

in the CIE $L^*a^*b^*$ colour coordinates (r) between the colour pixels of the lesion output and the linear model. The overall fitness is very high for such a simple model. Even in cases with lower correlations, we can observe that the model captures well the characteristics of the lesion output. For instance, the indoor scene for e_0 obtains $r = 0.81$, however, it can be appreciated that the linear model accounts well for the disappearance of red pixels in the lesion output. This is also evident in the kite picture of e_2 where blue pixels have vanished or the bench picture of e_5 with green pixels.

Naturally, there are limits to this linear modelling. For instance, the excess of chromaticity (pink and blue colours) in the indoor scene of e_6 is not fully captured by its linear model. The most extreme can be observed in the kite picture of e_3 for the $rgb2lab$ model (Figure 18) where the non-linear nature of lesion output is not accounted for in the linear model. Nevertheless, these parsimonious transformations reveal great details about the information encoded by each vector deserving more thorough investigation in future studies.

In Figure 20 we have illustrated the impact of each linear transformation applied to the entire RGB cube. This gives an intuitive idea of what each vector performs in a simple glance. Absence of some vectors results in the collapse of a chromatic direction. Others shear, shrink or expand the colour space.

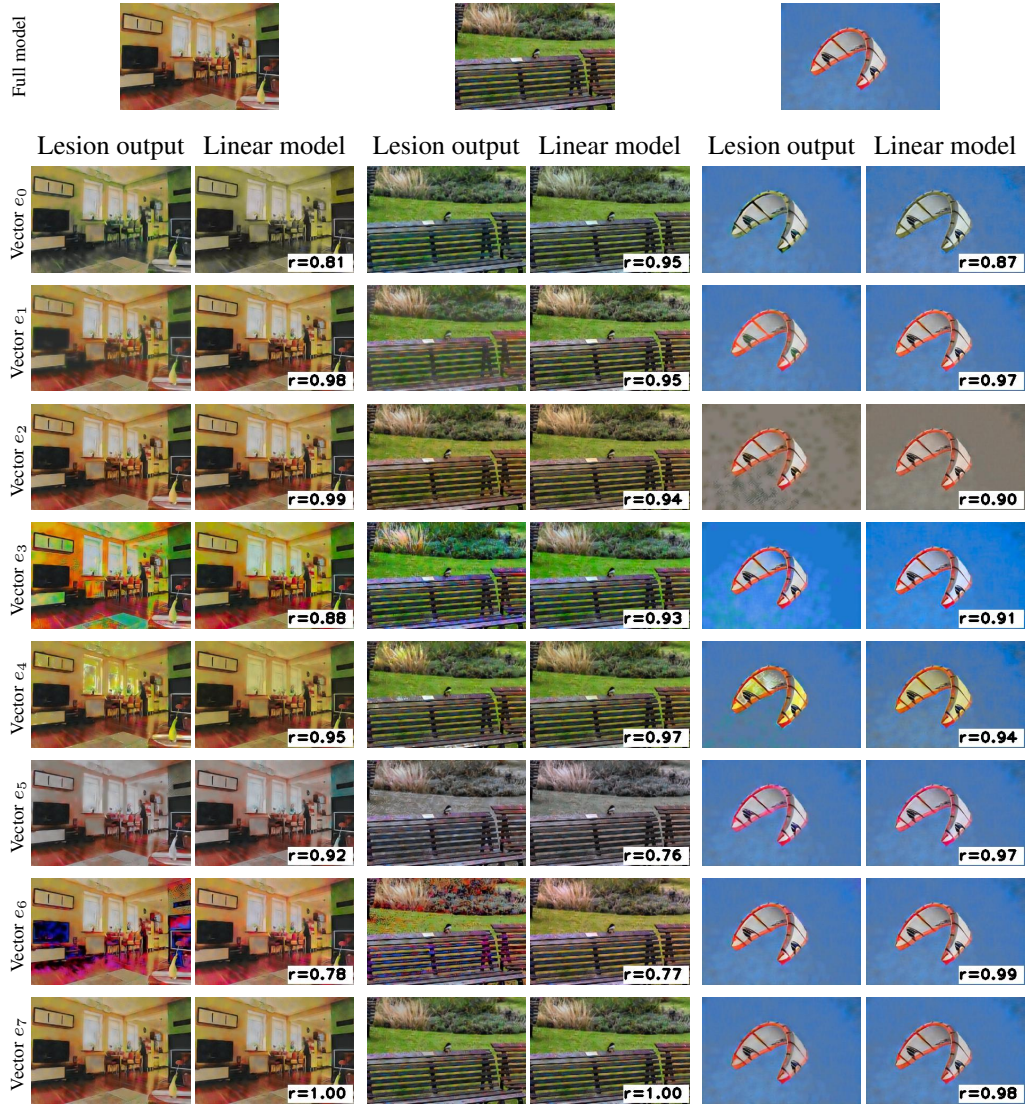


Figure 17: The linear modelling of vector lesion for *rgb2dkl* VQ-VAE of $K=8$ and $D=128$. The denoted r on the bottom right corner of an image is the measure of transformations' fitness.

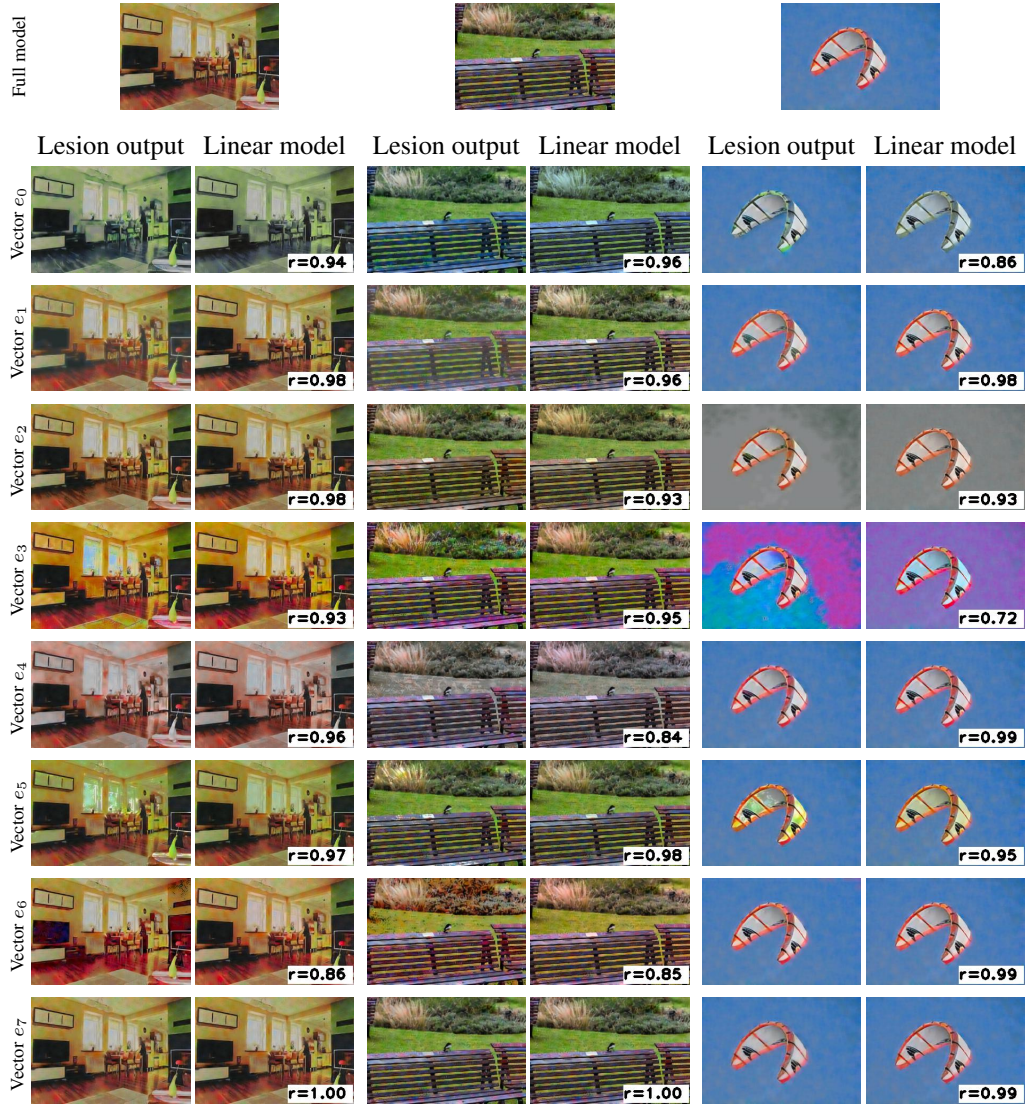


Figure 18: The linear modelling of vector lesion for *rgb2lab* VQ-VAE of $K=8$ and $D=128$. The denoted r on the bottom right corner of an image is the measure of transformations' fitness.

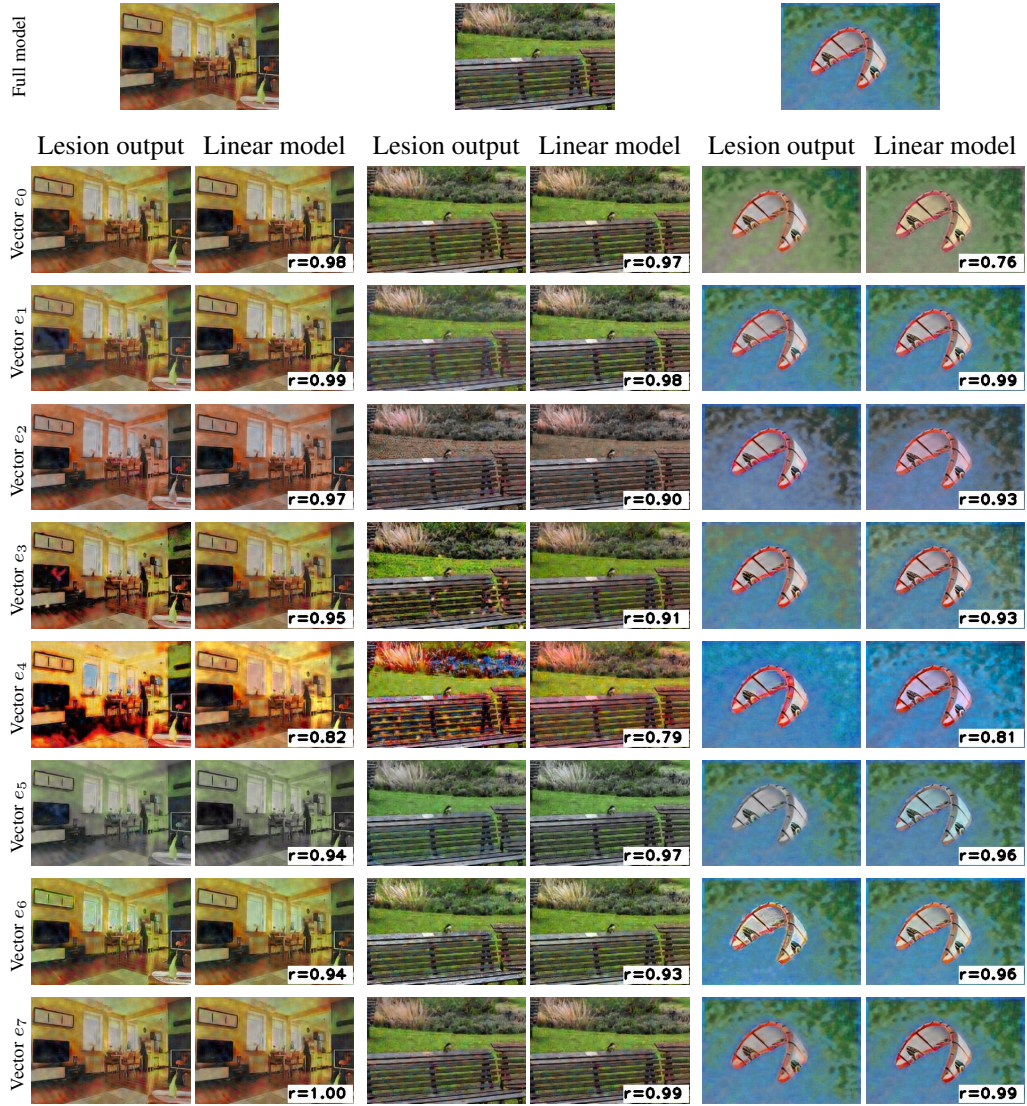


Figure 19: The linear modelling of vector lesion for *rgb2rgb* VQ-VAE of $K=8$ and $D=128$. The denoted r on the bottom right corner of an image is the measure of transformations' fitness.

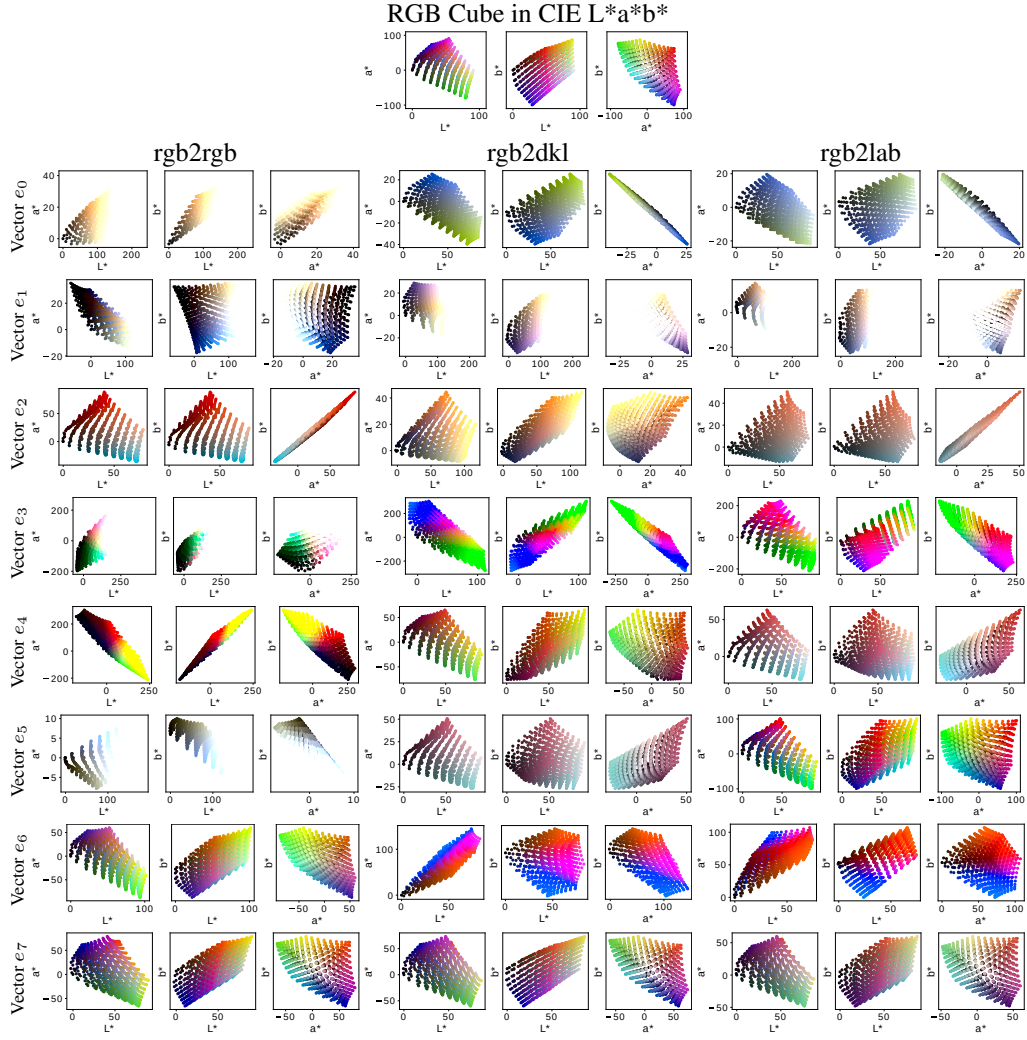


Figure 20: The impact of vector lesion on RGB cube plotted in CIE $L^*a^*b^*$ coordinate,